Water Research 198 (2021) 117134

Contents lists available at ScienceDirect

Water Research

journal homepage: www.elsevier.com/locate/watres

Compound-specific radiocarbon reveals sources and land–sea transport of polycyclic aromatic hydrocarbons in an urban estuary

Miaolei Ya[a,b,1], Yuling Wu[a,1], Li Xu[c], Yongyu Li[a], Hanzhe Chen[a], Xinhong Wang[a,*]

[a] State Key Laboratory of Marine Environmental Science, College of the Environment and Ecology, Xiamen University, Xiamen, China
[b] School of Environmental and Biological Engineering, Nanjing University of Science and Technology, Nanjing, China
[c] National Ocean Sciences Accelerator Mass Spectrometry Facility, Department of Geology and Geophysics, Woods Hole Oceanographic Institution, Woods Hole, MA, United States

ARTICLE INFO

Article history:
Received 7 November 2020
Revised 6 April 2021
Accepted 7 April 2021
Available online 11 April 2021

Keywords:
Compound-specific radiocarbon analysis
Perylene
Sediment
^{14}C signature
Coastal current
End-member mixing model

ABSTRACT

As typical chemical indicators of the Anthropocene, polycyclic aromatic hydrocarbons (PAHs) and their environmental behavior in urban estuaries can reveal the influence of anthropogenic activities on coastal zones worldwide. In contrast to conventional approaches based on concentration datasets, we provide a compound-specific radiocarbon (^{14}C) perspective to quantitatively evaluate the sources and land–sea transport of PAHs in an estuarine–coastal surficial sedimentary system impacted by anthropogenic activities and coastal currents. Compound-specific ^{14}C of PAHs and their ^{14}C end-member mixing models showed that 67–73% of fluoranthene and pyrene and 76–80% of five- and six-ring PAHs in the Jiulong River Estuary (JRE, China) originated from fossil fuels (e.g., coal, oil spill, and petroleum-related emissions). In the adjacent Western Taiwan Strait (WTS), the contributions of fossil fuel to these PAH groups were higher at 74–79% and 84–87%, respectively. Furthermore, as a significant biomarker for source allocation of terrigenous organic matter, perylene, a typical five-ring PAH, and its land–sea transport from the basin through the JRE and finally to the WTS was quantitatively evaluated based on the ^{14}C transport models. In the JRE, fluvial erosions and anthropogenic emissions affected the ^{14}C signature of perylene ($\Delta^{14}C_{perylene}$, -535 ± 5‰) with contributions of > 38% and < 62%, respectively. From the JRE to the WTS, the decreased $\Delta^{14}C_{perylene}$ (-735 ± 4‰) could be attributed to the long–range transport of "ocean current-driven" perylene (-919 ± 53‰) with a contribution of 53 ± 8%. This compound-specific ^{14}C approach and PAH transport model help provide a valuable reference for accurately quantifying land–sea transport and burial of organic pollutants in estuarine–coastal sedimentary systems.

1. Introduction

Anthropogenic activities have released large quantities of polycyclic aromatic hydrocarbons (PAHs) into the global environment (Tobiszewski and Namieśnik 2012), causing PAHs to be widely distributed in terrestrial ecosystems (Gregg, Prahl and Simoneit, 2015; Inomata et al., 2012). Therefore, PAHs are chemical signatures that can be used to mark the onset of the Anthropocene in an estuary (Bigus, Tobiszewski and Namieśnik, 2014; Leorri et al., 2014; Martins et al., 2011; Vane et al., 2011). Estuarine and coastal sediments are usually regarded as "sinks" for terrigenous PAHs, where they become preserved (Bianchi, Allison and Cai, 2013; Fontenelle et al., 2019; Liu et al., 2021; Sutilli et al., 2019). The concentrations, composition profiles, and diagnostic ratios of sedimentary PAHs and their geographical variations in estuarine–coastal systems are usually examined based on the concentration monitoring approach. This can provide the first insight into their origins, land–sea transport, and relative impacts of fluvial transport

Abbreviations: CSRA, compound-specific radiocarbon analysis; PAHs, polycyclic aromatic hydrocarbons; ^{14}C, radiocarbon; JRE, Jiulong River Estuary; WTS, Western Taiwan Strait; XM, Xiamen City; ZZ, Zhangzhou; JR, Jiulong River; TS, Taiwan Strait; ECS, East China Sea; SCS, South China Sea; MZCC, Min–Zhe Coastal Current; GC–MS, gas chromatography–mass spectrometry; TOC, total organic carbon; dw, dry weight; GC–FID, gas chromatography–flame ionization detector; PCGC, preparative capillary gas chromatography; PFC, preparative fraction collector; NOSAMS, National Ocean Sciences Accelerator Mass Spectrometry; WHOI, Woods Hole Oceanographic Institute; AMS, accelerator mass spectrometry; MDLs, method detection limits; Ace, acenaphthylene; Acen, acenaphthene; Flu, fluorene; Phen, phenanthrene; An, anthracene; Fluo, fluoranthene; Py, pyrene; BaA, benzo(a)anthracene; Chry, chrysene; BbF, benzo(b)fluoranthene; BjF, benzo(j)fluoranthene; BkF, benzo(k)fluoranthene; BaP, benzo(a)pyrene; IP, indeno(1,2,3-c,d)pyrene; DBA, dibenzo(a,h)anthracene; BgP, benzo(g,h,i)perylene; Per, perylene.

* Corresponding author. State Key Laboratory of Marine Environmental Science, Xiamen University, Xiamen, China.
E-mail address: xhwang@xmu.edu.cn (X. Wang).
[1] These authors contributed equally to this work.

https://doi.org/10.1016/j.watres.2021.117134
0043-1354/

(Wang et al., 2015; Wu et al., 2019a). However, the geochemical signals based on PAH concentration datasets can be modified during weathering processes in the environment due to selective losses in chemical/biological reactions, and thereby causing ambiguous PAH source results (Katsoyiannis, Sweetman and Jones, 2011; Ya et al., 2020; Zhang et al., 2005).

Radiocarbon (^{14}C, $t_{1/2}$ = 5730 ys) data, based on compound-specific radiocarbon analysis (CSRA), can characterize the sources and transport of ambient PAHs independent of their history regarding degradation conditions (Ingalls and Pearson 2005; Ya et al., 2018). In the past twenty years, an increasing amount of research has been devoted to exploring the source information in the ^{14}C signatures of PAHs (Bosch et al., 2015; Kumata et al., 2006; Sheesley et al., 2009; Tang et al., 2020; Zencak et al., 2007). Expanding the application of the ^{14}C signature as an indicator can provide an important reference for clarifying the transport and fate of organic pollutants at the land–sea interface.

In addition, CSRA can also provide information based on molecular-level ^{14}C analysis to further complement or validate the "traditional" use of the biomarkers as biogeochemical tracers (Eglinton et al., 1997). Perylene; a typical five-ring PAH; could potentially be used for source allocation of terrigenous organic matter in aquatic sediments (Hanke et al., 2019; Jiang et al., 2000; Zhang et al., 2014). Its origin shows a markedly different historical record from anthropogenic and natural PAHs, resulting in a longstanding debate in geochemical research and pollutant forensics (Bertrand et al., 2013; Grice et al., 2009; Hanke et al., 2019; Jiang et al., 2000; Marynowski et al., 2013; Varnosfaderany et al., 2014; Venkatesan 1988; Zhang et al., 2014). First, in contrast to other unsubstituted PAHs, combustion only produces trace or small amounts of perylene because of its extreme thermodynamic instability and higher reactivity (Bakhtiari et al., 2009; Grice et al., 2009; Jenkins et al., 1996). Second, perylene has been identified as a diagenetic product of wood-derived fungi (i.e., "terrigenous" production) in forest soils through isotopic tracing (Hanke et al., 2019; Silliman et al., 2000). Third, in marine sediments, perylene can be generated by microbially mediated in situ diageneses of organic carbon (Suzuki et al., 2010; Venkatesan 1988). Finally, fossil fuels (e.g., coal and crude oils) are also one of the sources of perylene in sediment (Grice et al., 2009; Jiang et al., 2000).

Although the sources of perylene have largely been clarified, the quantitative land–sea transport processes of perylene as a typical terrestrial biomarker have not been further studied. Based on the above-mentioned generation processes of perylene, a combination of soil and fluvial erosion (Hanke et al., 2019; Varnosfaderany et al., 2014), microbially mediated in situ diageneses (Suzuki, Yessalina and Kikuchi, 2010; Venkatesan 1988), and anthropogenic inputs (in particular, oil and coal spills in coastal cities and harbors) (Grice et al., 2009; Jiang et al., 2000) are the predominant sources of perylene in estuarine–coastal systems and collectively regulate the input, mixing, and burial of perylene. Therefore, considering the geochemical significance of perylene in the connectivity between terrestrial and marine ecosystems (Hanke et al., 2019), the compound-specific ^{14}C of perylene and the ^{14}C end-member mixing model can provide critical information for quantitatively evaluating the origins and land–sea transport of perylene from terrestrial systems through estuaries and to adjacent coasts.

The iulong river estuary (JRE) and adjacent western aiwan strait (WTS) is a representative subtropical estuarine–coastal system that is heavily impacted by anthropogenic activities and the East Asian monsoon (Wu et al., 2016; 2019a). Therefore, it can be used as a "natural laboratory" for studying the land–sea transport of perylene and other PAHs based on the expanded application of CSRA. In this study, we examined the concentrations, profiles, and ^{14}C contents of sedimentary PAHs as potential biogeochemical tracers to quantitatively reveal the influence of land–sea interactions. First, we assessed the impact of the land–sea interactions on the spatial heterogeneity of sedimentary PAHs. Second, as well as aiding in the source appointment of PAHs, the spatial ^{14}C variations of PAHs were used to track additional geochemical information such as the transport and fate of sedimentary PAHs. The compound-specific ^{14}C approach can help further clarify the environmental implication of PAH isotopes. Finally, based on the ^{14}C of perylene, we built a ^{14}C end-member mixing model to quantitatively evaluate the land–sea transport of perylene. Overall, this study provides a quantitative description of the origin and transport of perylene and other PAHs in an estuarine–coastal sedimentary system.

2. Materials and methods

2.1. Sediment sampling

Surface sediments from the JRE and WTS were collected onboard *R/V Haiyang 2* in May 2015, and *R/V Yanping 2* in June 2015, respectively. The sampling sites were divided into four regions: upstream JRE (JRE-U, A1 to A8, n = 6), downstream JRE (JRE-D, JY0-JY3, n = 4), WTS coast just north of the JRE (WTS-N, XA0-X5×01, X02, n = 7), and WTS coast just south of the JRE (WTS-S, X50-X73, n = 8) (Fig. 1). The top ~5 cm of sediment was collected at each sampling site using a stainless-steel grab sampler and then placed in pre-baked aluminum containers, sealed, and frozen at −20 °C until further analysis.

2.2. PAH concentration analysis

The pretreatment procedures for sedimentary PAHs have been described in detail in our previous paper (Cai et al., 2016). Briefly, the sediment samples were freeze-dried and then strained through an 80-mesh sieve. After adding excessive activated copper powder, 10 g of sediment was spiked with five deuterated PAH surrogates and then ultrasonically extracted using n-hexane/acetone (1:1, v/v) three times. After rotary evaporation, the concentrated extract was purified using pretreated alumina/silica gel chromatography (Text S1 of Supporting Information, SI). Finally, the eluate was evaporated to 100 μL under a gentle stream of N_2 gas (99.99% purity) and stored at −20 °C prior to instrumental analysis. PAHs were analyzed by gas chromatography–mass spectrometry (GC–MS) using an Agilent 6890 Series GC and an Agilent 5973 MS. Detailed instrumental conditions have been described in our previous papers (SI Text S1) (Ya et al., 2017a,2017b). The targeted compounds included 15 priority PAHs designated by the US EPA (without naphthalene) and perylene (m/z = 252). Their abbreviations are listed in Table S1. Sedimentary total organic carbon (TOC) concentrations were analyzed using a Vario EL-III Elemental Analyzer; the procedures are described in detail in our previous paper (Wu et al., 2019b). The reported PAH and TOC concentrations were based on dry weight (dw).

2.3. Bulk sample preparation for ^{14}C analysis

To satisfy the carbon content required for $\Delta^{14}C$ measurements of PAHs, we combined equivalent amounts of sifted sediments from all the JRE stations (680 g total, sites A1 to A8 and JY0-JY3) and equivalent amounts of sediments from all the WTS stations (620 g total, sites XA0-X5×01, X02, and X50-X73) into two bulk samples (named JRE and WTS). The pretreatment flow diagram for the $\Delta^{14}C$ measurements of the targeted PAHs in the sediments is shown in Fig. S1. Sediment samples were freeze-dried and strained through an 80-mesh sieve. After adding excessive activated copper powder, the sediments were ultrasonically extracted with dichloromethane/methanol (9:1, v/v) three times. The extracts

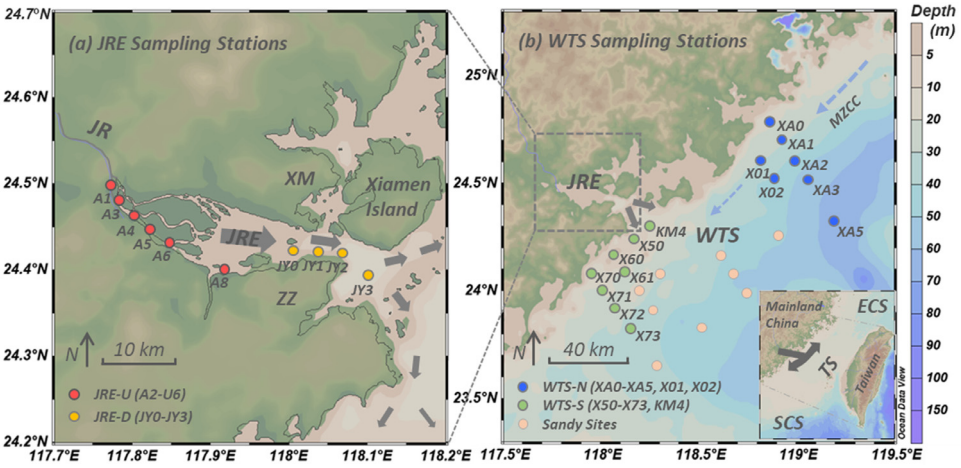

Fig. 1. Sampling regions and stations in (a) the Jiulong River Estuary (JRE) and (b) the Western Taiwan Strait (WTS). Xiamen City (XM); Zhangzhou City (ZZ), Jiulong River (JR); Taiwan Strait (TS); East China Sea (ECS); South China Sea (SCS); Min–Zhe Coastal Current (MZCC).

were combined, evaporated to 10 mL, and then saponified with 10 mL of a 0.5 mol L^{-1} KOH solution in methanol/water (4:1, v/v) for 2 h at 80 °C. The neutral fraction containing PAHs was extracted with *n*-hexane three times, and was evaporated to ~1 mL before being chromatographically separated in a glass column packed with activated silica gel (activated at 500 °C for 4 h and deactivated with 5% water). The elution solvents were *n*-hexane and *n*-hexane/dichloromethane (1:1, v/v). The *n*-hexane/dichloromethane phase containing PAHs was evaporated to ~1 mL, cleaned by partitioning with *n*-pentane/dimethylformamide, dried with anhydrous sodium sulfate (Mandalakis, Zebühr and Gustafsson, 2004b; Ya et al., 2018), and reduced to ~0.5 mL with a gentle stream of N_2. Chromatograms of the gas chromatography–flame ionization detector (GC–FID) before and after purification by *n*-pentane/dimethylformamide are shown in Fig. S2.

After chemical purification, preparative capillary gas chromatography (PCGC) was used to isolate and prepare the targeted PAHs for CSRA. We presented the details of the PCGC procedure in a previous paper (Text S2) (Ya et al., 2018). In this study, targeted PAHs were initially separated using an Agilent J&W HP-5 ms column (60 m length; 0.53 mm i.d.; film thickness, 0.25 μm) and collected using a preparative fraction collector (PFC). The initially prepared PAHs were combined and subjected to a second separation step using an Agilent J&W DB-17 ms polar column (30 m length; 0.32 mm i.d.; film thickness, 0.25 μm) and were again collected by the PFC. After being trapped, the targeted PAHs were transferred to 4 mL vials after rinsing with *n*-pentane four times. Finally, the samples were passed through a silica gel column to remove the column bleed. A small aliquot was taken from each trap to check the purity of the targeted PAHs using a GC–FID equipped with a high-resolution Agilent J&W VF-5 ms column (25 m length; 0.2 mm i.d.; film thickness, 0.33 µm). Limited by the sample size of the individual PAHs, we utilized the sum of phenanthrene and anthracene (Phen + An), fluoranthene and pyrene (Fluo + Py), five- and six-ring PAHs (including benzo(*b* + *j* + *k*)fluoranthene, benzo(*a*)pyrene, indeno(1,2,3-*c,d*)pyrene, dibenz(*a,h*)anthracene, and benzo(*g,h,i*)perylene), and perylene (Per) as the four targeted PAH groups for ^{14}C analysis. The final chromatograms of the targeted PAHs from the JRE and WTS are shown in Fig. S3.

$\Delta^{14}C$ analysis of TOC in the surface sediments of the JRE and WTS was also performed at the national ocean sciences accelerator mass spectrometry (NOSAMS) facility of woods hole oceanographic institute (WHOI). The following "offline combustion" and graphite preparation processes for $\Delta^{14}C$ measurement were conducted at the NOSAMS facility at WHOI (Pearson et al., 1997). Briefly, after catalytic oxidation of the targeted PAHs and TOC, the generated CO_2 was purified and quantified in the vacuum glass line and reduced to graphite. Finally, $\Delta^{14}C$ was measured by accelerator mass spectrometry (AMS) at the NOSAMS facility (Pearson et al., 1997). The detailed procedures have been presented in Shah and Pearson (2007) and Xu et al. (2012). The reported $\Delta^{14}C$ values, based on the sampling year, were compared to the NBS oxalic acid I (NIST SRM 4990) standard after normalizing the radiocarbon content of a sample to the same $\delta^{13}C$ value (−25‰) and year (1950) (Stuiver and Polach 1977).

2.4. Quality assurance and control

The analytical procedures were carefully performed to ensure quality control. Six laboratory blanks were measured to monitor potential contamination during sample handling in the laboratory. The PAH concentrations in the lab blank samples were ~2 orders of magnitude lower than those in the samples (based on a sample weight of 10 g dw, *see* Table S2), indicating that the background PAHs from the laboratory could be largely ignored. Deuterated surrogate standards were used to correct for losses that occurred during the pretreatment procedures. PAH recoveries ranged from 60–120%, with a mean of 97 ± 19% (Table S2). The method detection limits (MDLs) were calculated as the mean plus three times the standard deviation of the lab blanks (Rauert et al., 2020). If an analyte was not detected in the blanks, the concentration of a peak with a signal-to-noise ratio of 10:1 was inserted for MDLs (Rauert et al., 2020). The MDLs of PAHs ranged from 0.01–1.04 ng g^{-1} dw, with a mean of 0.27 ± 0.32 ng g^{-1} dw (Table S2).

For the ^{14}C analysis of bulk samples, PAH and external carbon contamination was avoided throughout the entire process. All glassware, aluminum foil, and anhydrous sodium sulfate were baked at 500 °C for 4 h prior to use. Detailed quality assurance procedures are described in our previous paper (Ya et al., 2018). Briefly, the concentration of PAHs in process blanks of extraction and purification procedures was ~2 orders of magnitude lower than that of field samples (Table S2). During the PCGC process, deviations in retention times were strictly controlled to avoid the introduction of impure components and isotope fractionation of the targeted PAHs (Xu et al., 2012; Ya et al., 2018). We employed column bleed removal steps to avoid additional carbon contamination from the stationary phase. The solvent (*n*-pentene) used in the column bleed removal step was blown to dryness in a baked quartz tube. Finally, the estimated purities of the isolated PAHs based on

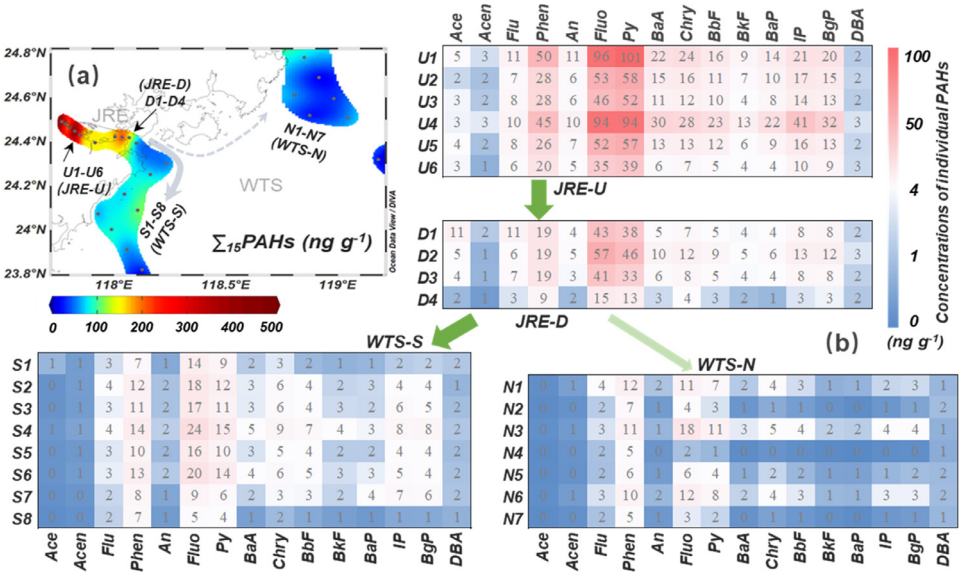

Fig. 2. (a) Contour map of the distribution of total polycyclic aromatic hydrocarbon (PAH) concentrations (Σ_{15}PAHs, ng g^{-1} dw) in the Jiulong River Estuary (JRE) and Western Taiwan Strait (WTS); (b) heat map showing the concentration variations of 15 PAHs (ng g^{-1} dw) from the JRE to the WTS.

the chromatogram (as determined by GC–FID) ranged from 90–100% (Table S3). Overall, the quality assurance measures satisfied the small sample (< 2 μmol) ^{14}C test requirements of the NOSAMS facility at WHOI (Pearson et al., 1997). For reference, we report the carbon impurity-corrected Δ^{14}C results based on the assumption that all impurities were derived from fossil or modern carbon. Detailed procedures and results are given in SI Text S3 and Table S3, respectively. The statistical analysis method is introduced in SI Text S4.

3. Results and discussion

3.1. Spatial heterogeneity of sedimentary PAHs

The total concentrations of the 15 US EPA-designated priority PAHs in surface sediments of the JRE and WTS ranged from 14–452 (126 ± 116) ng g^{-1} dw, with a median concentration of 75 ng g^{-1} dw (Fig. 2 and Table S4). Fluo (ranging from 1.8–96 ng g^{-1} dw with median and mean concentrations of 18 and 28 ± 26 ng g^{-1} dw, respectively), Py (range = 1.5–101, median = 12, mean = 26 ± 28 ng g^{-1} dw), followed by Phen (range = 5.3–50, median = 12, mean = 16 ± 12 ng g^{-1} dw) were present in the highest relative abundances, with mean percent contributions to the total PAHs of 22 ± 3.6%, 18 ± 4.7%, and 16 ± 6.9%, respectively (Table S4 and Fig. S4).

The amounts of these three PAHs in the JRE–WTS sedimentary system were higher than those in the continental shelf sediments of China (Fluo: 8.0; Py: 6.4; Phen: 11 ng g^{-1} dw) (Liu et al., 2012) and the Amazon coastal zone (Fluo: 3.7; Py: 4.1; Phen: 2.9 ng g^{-1} dw) (Pichler et al., 2021); close to the levels found in the Mediterranean lagoon in the Northern Adriatic Sea, Italy (Fluo: 59; Py: 33; Phen: 21 ng g^{-1} dw) (Acquavita et al., 2014), the estuarine sediments over China (Fluo: 25; Py: 14; Phen: 40 ng g^{-1} dw in dry season; Fluo: 15; Py: 6; Phen: 19 ng g^{-1} dw in wet season) (Li et al., 2021), and the Knysna Estuary, South Africa (Fluo: 39; Py: 32; Phen: 35 ng g^{-1} dw) (Liu et al., 2021); and lower than those found in the Lenga estuary, central Chile, and the South Pacific (Fluo: 356; Py: 342; Phen: 142 ng g^{-1} dw) (Pozo et al., 2011). In total, sedimentary PAHs in the JRE and WTS were at relatively low or moderate levels compared with other estuarine and coastal regions worldwide (Acquavita et al., 2014; Li et al., 2021; Liu et al., 2012,2021); Pichler et al., 2021; Pozo et al., 2011). Compared with two decades ago, PAH concentrations in the JRE have gradually decreased and their composition has dramatically changed (Maskaoui et al., 2002; Zhang et al., 2000), which partly reflects changes in energy efficiency, frequent utilization of cleaning technologies, and emission controls (Lu et al., 2019).

As a typical class of environmental tracers, the spatial heterogeneity of surface sedimentary PAHs can provide an insight into the short-term influence of the river on the estuary and coast. In the JRE–WTS system, PAH concentrations decreased by several to ten times from the estuary to the coastal areas (Fig. 2 and Table S4), as reported in the western South Atlantic upper continental margin (Santos et al., 2020). Both total and individual PAH concentrations (especially the predominant Fluo, Py, and Phen) showed significant negative correlations with the offshore distance (km) from the JRE towards the WTS ($p < 0.01$, Spearman's rank) (Table S5). PAHs also showed a significant positive correlation with TOC concentrations (Table S4) in JRE-WTS sedimentary system ($p < 0.01$, Spearman's rank). This revealed that fluvial transport by hydrodynamic forces was one of the crucial driving forces of sedimentary PAH distribution, along with surface runoff (Lin et al., 2013; Ya et al., 2018). During transport into the estuary and sea, PAHs are dispersed, degraded, and finally buried in the estuarine–coastal sedimentary system (Liu et al., 2012; Wang et al., 2015). In contrast to decreased concentrations, the percentages of PAH species were relatively constant from upstream to downstream reaches, and finally to WTS-S, with differences seen at WTS-N (Fig. S4). The decreasing concentration and constant composition can partly reflect the stronger influence of JRE-diluted water on the southern coast of the WTS than on the northern coast over the past decade (the time scale can be calculated by the sampling depth of ~5 cm and a mean linear sedimentation rate of > 0.4 cm $year^{-1}$; Huh et al., 2011).

Besides the JRE, long-range alongshore transport of river-derived materials from the Yangtze River and other coastal rivers (such as the Qiantang, Ou, and Min Rivers) driven by the Min–Zhe coastal current (MZCC) (Hu et al., 2014) could be another significant factor affecting the spatial heterogeneity of sedimentary PAHs

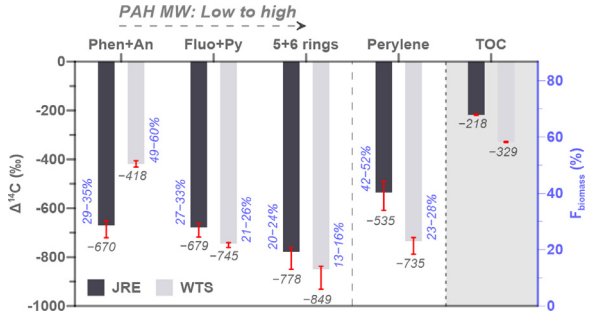

Fig. 3. $\Delta^{14}C$ values (‰) of targeted polycyclic aromatic hydrocarbons (PAHs) determined by compound-specific radiocarbon analysis (CSRA) in surface sediments and the corresponding fractional contributions (%) from biomass burning from the Jiulong River Estuary (JRE) and Western Taiwan Strait (WTS). Columns represent measured $\Delta^{14}C$ values and red lines represent $\Delta^{14}C$ ranges of PAHs after correcting for carbon impurities (SI Text S3 and Table S3). Molecular Weight (MW); Total organic carbon (TOC).

in coastal WTS (Lin et al., 2013; Ya et al., 2018). Previous studies have revealed that the MZCC can substantially affect the balance of black carbon and PAH budgets of the coastal WTS (Li et al., 2016; Wu et al., 2019b). Overall, the spatial heterogeneity of both PAH concentrations and compositions can reflect regional differences in the intensity of land–sea interactions of terrigenous PAHs and also be used as auxiliary evidence from the perspective of sedimentary PAHs for determining regional short-term average deposition characteristics of the river plume discharging into the WTS (Wang, Zheng and Hu, 2013).

3.2. Sources and transport of PAHs determined by their ^{14}C signatures

The ^{14}C signatures of individual PAHs were measured to identify their sources and transport from the estuary to adjacent coasts. Based on the available carbon masses of the compounds (Table S3), $\Delta^{14}C$ measurements were performed on four groups of combined PAHs (Phen + An, Fluo + Py, Perylene, five- + six-ring PAHs). The total amounts of carbon in the corresponding PAH samples available for $\Delta^{14}C$ analysis ranged from 2.1 – 6.0 μmol C, and the purities of the isolated PAH groups ranged from 90–100% (Table S3). Overall, the measured $\Delta^{14}C$ values of Phen + An ($\Delta^{14}C_{Phen\&An}$) were -670 ± 5‰ and -418 ± 5‰; Fluo + Py ($\Delta^{14}C_{Fluo\&Py}$) were -679 ± 5‰ and -745 ± 5‰; and five- + six-ring PAHs ($\Delta^{14}C_{5+6\ rings}$) were -778 ± 3‰ and -849 ± 3‰, in the JRE and WTS, respectively (Fig. 3 and Table S3). As a reference, the carbon impurity-corrected $\Delta^{14}C$ results are also listed in Table S3 and shown in Fig. 3.

The global comparison of ^{14}C signatures of PAHs in sediment can reflect the source differences of buried PAHs derived from the surrounding anthropogenic activities (Ya et al., 2020). The ^{14}C signatures of the targeted PAHs in the surface sediments of the JRE–WTS system are comparable to those in sediment cores from Siskiwit Lake located on Isle Royale, Michigan (−783‰ to −388‰) (Slater et al., 2013) and in surface sediments from the waterways of the Stockholm metropolitan area (−934‰ to −585‰) (Mandalakis et al., 2004a). These values are much higher than those reported in sediment cores from the Peace–Athabasca Delta, in the vicinity of the rapidly developing oil sand industry in Northern Alberta, Canada (−962‰ to −849‰) (Jautzy et al., 2015), and those from an urban reservoir located in the central Tokyo metropolitan area, Japan (−934‰ to −824‰) (Kanke et al., 2004).

Moreover, the ^{14}C signatures of TOC (i.e., $\Delta^{14}C_{TOC}$) were −218‰ and −329‰ in the JRE and WTS, respectively (Fig. 3 and Table S3), which are comparable to those in the adjacent areas reported by Bao et al. (2016). These $\Delta^{14}C_{TOC}$ values were also much higher than the targeted PAHs in the JRE and WTS (Fig. 3). This is not surprising, as a higher proportion of "modern carbon" components was expected in the TOC pool, such as inputs from terrestrial higher plants (Li et al., 2017).

Furthermore, we estimated the fractional contributions of PAHs from biomass burning (C3 and C4 plants, $f_{biomass}$) and fossil fuels (coal combustion and petroleum-related emissions, $f_{fossil} = 1 - f_{biomass}$) using a ^{14}C end-member mixing model of PAHs expressed as $\Delta^{14}C_{PAH} = \Delta^{14}C_{biomass} \times f_{biomass} + \Delta^{14}C_{fossil} \times (1 - f_{biomass})$ (Jautzy et al., 2015; Tang et al., 2020; Xu et al., 2012; Ya et al., 2018). The $\Delta^{14}C$ value of the fossil fuel end-member ($\Delta^{14}C_{fossil}$) was −1000‰ (Xu et al., 2012). There were at least two components of the biomass burning signature (i.e., $\Delta^{14}C_{biomass}$). One was the wood-burning of perennial trees with a $\Delta^{14}C$ value of 225‰ that grew over the past 30–50 years in an atmosphere with elevated ^{14}C contents (Mandalakis et al., 2005; Zencak et al., 2007). The second was from the burning of materials produced during the current year, such as leaves and annual grass, i.e., $\Delta^{14}C$ of contemporary CO_2, which had a mean value of −8.7‰ around Xiamen City in 2014—as reported by Niu et al. (2016). These two components represent the maximum and minimum values of the modern end-member in the environment, respectively. In this study, we used these end-members to estimate the ranges of fractional contributions of PAHs from biomass burning and fossil fuels in the JRE and WTS (Table S3).

According to the ^{14}C end-member mixing model, the calculated fractional contributions from biomass burning of Phen + An, Fluo + Py, and five- + six-ring PAHs were 29–35%, 27–33%, and 20–24%, respectively, in the JRE and 49–60%, 21–26%, and 13–16%, respectively, in the WTS (Fig. 3 and Table S3). This is closer to the contribution rate of biomass sources (23%) to sedimentary black carbon in the East China Sea (Wang, 2020). Correspondingly, fossil fuel sources ($f_{fossil} = 1 - f_{biomass}$) contributed 65–71% of Phen + An, 67–73% of Fluo + Py, and 76–80% of five- + six-ring PAHs in the JRE, and 40–51%, 74–79% and 84–87%, respectively, in the WTS. Due to the high contemporary anthropogenic activity-derived emissions from surrounding cities and harbors (e.g., industry, shipping, traffic, and oil spills), anthropogenic fossil fuel-derived PAHs (including direct input and combustion processes of oil and coal) are the predominant contributor to PAHs in the JRE and WTS (Ya et al., 2018).

Interestingly, the contributions of fossil fuels to PAHs in sediments were lower than the contributions of fossil fuels to PAHs in the adjacent surface seawater (> 89%) reported in our previous work (Ya et al., 2018). In this study, surface sediments (top 5 cm) reflected the burial of PAHs over the past decade (Huh et al., 2011), whereas the surrounding surface seawater only represented the transitory PAH sources during the sampling period in our previous study. Therefore, the discrepancy in the proportion of fossil fuel-derived PAHs between sediment and surface seawater indirectly reflects the gradual increase in fossil fuel consumption along with rapid urbanization (Chen, Teng and Wang, 2012; Zhang and Lin 2012).

At the molecular level, $\Delta^{14}C$ values showed a decreasing trend with increasing PAH molecular weight (Phen + An > Fluo + Py > five- + six-ring PAHs) in both the JRE and WTS (Fig. 3). This reflects a decrease in biomass-sourced PAHs or an increase of fossil fuel-derived PAHs (e.g., coal and petroleum-related emissions) as the molecular weight increases. Spatially, $\Delta^{14}C_{Fluo\&Py}$ and $\Delta^{14}C_{5+6\ rings}$ values decreased during transport from the JRE to the WTS, which was consistent with the decreasing $\Delta^{14}C$ values of TOC from −218‰ to −329‰ (Fig. 3). Because of the high sedimentation rate (~0.4 cm year^{-1}) (Huh et al., 2011), the lower $\Delta^{14}C$ values of PAHs in the surface sediments of the WTS could not have been caused by in situ ^{14}C decay during long-term burial. There-

fore, we deduce that the lower ^{14}C contents of PAHs and TOC along the coast compared to the estuary can be attributed to a combination of three factors: (1) dilution/weakening of estuarine inputs (Wu et al., 2019a), (2) atmospheric contribution (Fang et al., 2016; Wu et al., 2019b; Yu et al., 2018), and (3) ocean current-driven inputs (Wu et al., 2013; Ya et al., 2017a, 2018). Undoubtedly, the decreasing PAH concentrations (Fig. 2) reflect the continued decreasing impact of the JRE-diluted water on the WTS. In addition, the high contribution of atmospheric deposition to the burial of black carbon in the WTS (Wu et al., 2019b) also reflects the non-negligible impact on the co-migration of PAHs (Fang et al., 2016). The fossil fuel-dominated aerosol inputs to China's marginal seas (Yu et al., 2018) means that atmospheric deposition could input a small percentage of low ^{14}C PAHs into the coastal environment (Ya et al., 2018). For ocean current-driven inputs, the long-range horizontal transport of coastal organic matter driven by the MZCC also carries lower ^{14}C contents of PAHs (Ya et al., 2018) and lower ^{14}C contents of TOC ($\Delta^{14}C$: -431 ± 29‰ in the inner shelf of the East China Sea; Wu et al., 2013). In contrast, the much lower ^{14}C content of Phen + An in the JRE than in the WTS (Fig. 3) may be related to releases of petroleum and its degradation products from Xiamen and Zhangzhou Harbors, which may contribute more fossil-Phen (a biomarker of petroleum residue; Fang et al., 2016).

Conventionally, diagnostic ratios of PAHs have been widely used to distinguish potential sources of PAHs in marine environments (Tobiszewski and Namieśnik 2012; Wu et al., 2011; Yunker et al., 2002). Because of the selective degradation of PAH isomers during the transport of PAHs and final burials into the sediment (Zhang et al., 2005), the degradation differences of the isomers should be fully considered to identify the sources of PAHs (Ya et al., 2017b). From the JRE to WTS, the decreased ratios of An/(An+Phen) and BaA/(BaA+Chry) and the increased ratios of Fluo/(Fluo+Py) (Fig. S5) were in line with their degradation half-life in the environment (Lu et al., 2005). This reflected the continuous degradation occurrence of PAHs from the estuary to coasts. However, the decrease in the ratios of IP/(IP+BgP) contradicted the fact that IP has a longer half-life than BgP (Tobiszewski and Namieśnik 2012). The unforeseen degradation degree of PAH isomers is one of the most important factors that cause the uncertainty of the diagnostic ratios in source identification of PAHs (Ya et al., 2018, 2020). However, the source identification of PAHs by CSRA shows its effectiveness in avoiding the uncertainties of degradation factors (Ya et al., 2020). Our previous study also emphasized the significant advantages in the quantitative source apportionment of PAHs compared with other approaches (e.g., diagnostic ratios and receptor models) (Ya et al., 2020).

3.3. Land–sea transport of sedimentary perylene: concentrations, ^{14}C contents, and end-member mixing models

As an important terrigenous biomarker (Varnosfaderany et al., 2014), perylene and spatial variations in its concentration and ^{14}C content can reflect changes in terrigenous inputs from rivers to coasts (Varnosfaderany et al., 2014; Ya et al., 2017b). From the JRE to the WTS, concentrations of sedimentary perylene gradually decreased from 183 to 3.6 ng g^{-1} dw, with mean concentrations of 125 ± 33, 86 ± 12, 52 ± 29, and 35 ± 28 ng g^{-1} dw in the JRE-U, JRE-D, WTS-S, and WTS-N, respectively (Fig. 4a, 4b, and Table S4). These values are comparable to those of previous studies on the estuarine–inner shelf of the Yangtze estuarine area (4.2–186.4 ng g^{-1} dw) and the East China Sea (7.4–141.1 ng g^{-1} dw, with a mean of 86.3 ± 34.7 ng g^{-1} dw) (Bouloubassi, Fillaux and Saliot, 2001; Hu et al., 2014). Furthermore, perylene concentrations were proportional to the overall amount of terrigenous inputs and showed a significant decreasing trend with increasing distance from the JRE to WTS ($r = -0.80$, $p < 0.01$) (Fig. 4a). A negative relationship

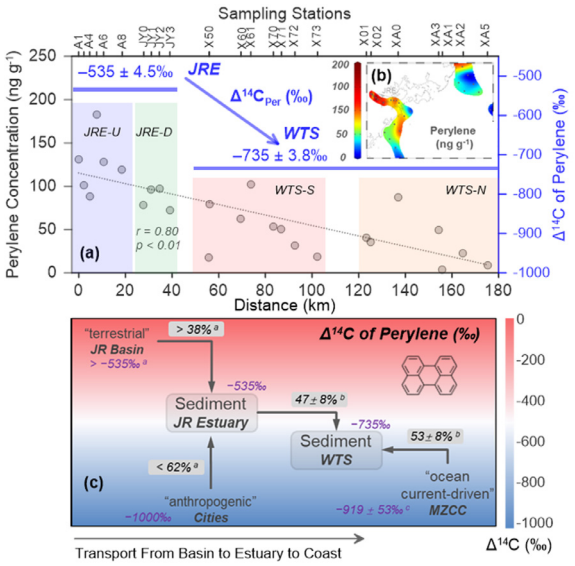

Fig. 4. (a) Spatial variations in concentrations (ng g^{-1} dw) and $\Delta^{14}C$ values (‰) of sedimentary perylene with offshore distance (km); (b) contour map of perylene (Per) concentrations (ng g^{-1} dw); and (c) land–sea transport model basing on ^{14}C end-member mixing model of perylene from the Jiulong (JR) basin, through the Jiulong River Estuary (JRE), and finally to the Western Taiwan Strait (WTS). [a] fractional contributions of "terrigenous" and "anthropogenic" perylene (two ends) were calculated by the ^{14}C mixing model of perylene in the JRE (*see* equations (2), (3) and (4) in SI Text S5); [b] fractional contributions of perylene from the JRE and the Min–Zhe Coastal Current (MZCC) (two ends) were calculated by the ^{14}C mixing model of total organic carbon (TOC) in the WTS (*see* equations (5) and (6) in SI Text S5); and [c] $\Delta^{14}C$ values of perylene from the MZCC were calculated by the ^{14}C mixing model of perylene in the WTS (*see* equation (7) in SI Text S5).

between perylene levels and transport distances from the estuary to the coasts has also been found in previous studies (Jiang et al., 2000; Ya et al., 2017b).

Perylene was a major PAH component in surface sediments from both the JRE and WTS (Table S4). Compared with other unsubstituted PAHs, the combustion process can only produce trace or small amounts of perylene owing to its thermodynamic instability and higher reactivity (Bakhtiari et al., 2009; Grice et al., 2009; Jenkins et al., 1996). Conventionally, when the percentage of perylene relative to total unsubstituted PAHs is > 4%, and that relative to five-ring PAHs (m/z = 252) is > 10%, the origin of perylene is usually thought to be biogenic or diagenetic (Varnosfaderany et al., 2014). In the JRE–WTS sedimentary system, perylene represented 20–62% (with a mean of 39 ± 10%) of total unsubstituted PAHs and 70–93% of five-ring PAHs (with a mean of 82 ± 6.0%) (Table S4). These diagnostic ratios, which are far above the above-mentioned thresholds, reflect the predominance of biogenic or diagenetic perylene and its precursors, which most likely originated from the following: (1) terrigenous inputs via surface runoff (Hanke et al., 2019; Varnosfaderany et al., 2014), (2) in situ diagenesis of organic carbon by microbial communities in the ocean (Suzuki, Yessalina and Kikuchi, 2010; Venkatesan 1988), and (3) petroleum from unintentional oil spills (Grice et al., 2009; Jiang et al., 2000).

From the perspective of radiocarbon values, the measured $\Delta^{14}C_{Per}$ values decreased from -535 ± 5‰ to -735 ± 4‰ from the JRE to the WTS (Fig. 4a and Table S3). The carbon impurity-corrected $\Delta^{14}C_{Per}$ values ranged from −617‰ to −485‰ and −791‰ to −720‰ in the JRE and WTS, respectively. The decreasing $\Delta^{14}C_{Per}$ and $\Delta^{14}C_{5+6\ rings}$ (Fig. 3) accompanied by the decreasing concentrations (Table S4) collectively indicated a decrease in the input intensity of land-based PAHs or ^{14}C dilution by in situ perylene production. The ^{14}C contents of perylene in the JRE and WTS

were higher than those in sediment cores from Northern Alberta, Canada (−873‰) (Jautzy et al., 2015) and lower than those in sediment cores from Siskiwit Lake on Isle Royale, Michigan (−296‰ to −199‰) (Slater et al., 2013). The regional differences in $\Delta^{14}C_{Per}$ values reflect the differences in the carbon age of its precursors, generation conditions, and aging time.

To further quantitatively evaluate the sources and land–sea transport intensity of surficial sedimentary perylene from the Jiulong (JR) basin through the JRE and finally to the WTS, we built a ^{14}C end-member mixing model of perylene in connection with geography and hydrodynamics (Fig. 4c). In the JRE, diagenetic products of soil-derived fungi carried by fluvial erosion from the JR basin were one of the predominant sources of sedimentary perylene (Fig. 4c). We defined this source (or end) as "terrigenous" and expressed its ^{14}C content as $\Delta^{14}C_{terr}$. Fossil fuels (e.g., coal and crude oils) (Grice et al., 2009; Jiang et al., 2000) from cities (especially the harbors) were another predominant source of perylene in the JRE (Fig. 4c). We defined this as an "anthropogenic" source (or end) caused by anthropogenic activities, and its ^{14}C content was expressed as $\Delta^{14}C_{anth}$, i.e., $\Delta^{14}C_{fossil}$. These two appointed ends, i.e., "terrigenous" and "anthropogenic," are also consistent with the biogenic or diagenetic indication deduced by the much higher ratios of perylene concentrations to total unsubstituted PAH and fivering PAH concentrations mentioned above.

Based on the above description, fractional contributions of the "terrigenous" (f_{anth}) and "anthropogenic" (f_{anth}) sources to sedimentary perylene in the JRE can be expressed as $f_{terr} = (1 + \Delta^{14}C_{JRE\text{-}Per})/(1 + \Delta^{14}C_{terr})$ and $f_{anth} = 1 - f_{terr}$, respectively (for the detailed calculation process, please *see* equations (2), (3), and (4) in SI Text S5). According to this expression, we can further deduce that the mean $\Delta^{14}C_{terr}$ value of perylene from fluvial erosion of the JR basin is larger than the $\Delta^{14}C_{Per}$ value in the JRE, i.e., $\Delta^{14}C_{terr} > \Delta^{14}C_{JRE\text{-}Per} = -535‰$ (Fig. 4c), and the corresponding ^{14}C ages is < 6087 yr. A previous study in a forest-covered stream in the Pettaquamscutt River basin, Rhode Island, also reported much lower $\Delta^{14}C_{Per}$ values of −255‰ to −78‰ (Hanke et al., 2019). This pre-aged perylene also indicates a diagenetic product of wood-derived fungi in soils (Grice et al., 2009). If we took the $\Delta^{14}C$ value of 225‰ for perennial trees that grew over the past 30–50 years as the upper line of the $\Delta^{14}C_{terr}$ value (Mandalakis et al., 2005; Zencak et al., 2007), the ranges of f_{terr} from the JR basin should be > 38%, and the corresponding ranges of f_{anth} should be < 62% (Fig. 4c).

Estuarine input is an important source of perylene in offshore sediment (Ya et al., 2017b). Regarding the variation of the ^{14}C signature of perylene from the JRE (-535 ± 5‰) to the WTS (-735 ± 4‰), in situ ^{14}C decay of post-depositional perylene in surface sediments is not possible on the short timescales of fluvial transport (Huh et al., 2011). There is evidence that long-range alongshore transport of the MZCC plays an important role in conveying pollutants to the coastal sediments of the WTS (Hu et al., 2014; Liu et al., 2018; Wu et al., 2019b), similar to the lateral movement of old sediments along the shelf judged by radioisotopic tracers (Santschi et al., 2001). Meanwhile, continued generation of perylene during long-range transport also occurs by microbially mediated diagenesis from precursors (Silliman et al., 2000). Therefore, a combination of long-range transport by the MZCC and accompanying microbially mediated in situ diageneses of perylene, collectively referred to as "ocean current-driven inputs," was another factor that affected the ^{14}C signature of perylene in the WTS.

Based on the above discussion, "discharge from the JRE" and "the ocean current-driven inputs" predominantly by the MZCC (defined as $\Delta^{14}C_{MZCC}$), were the two predominant sources of sedimentary perylene in the WTS, and can be defined as $\Delta^{14}C_{JRE\text{-}Per}$ and $\Delta^{14}C_{MZCC\text{-}Per}$, respectively. In addition, we found a significant positive correlation between the perylene and TOC concentrations ($r = 0.86$, $p < 0.01$, Table S5). Many other studies have also observed similar relationships between the concentrations of perylene and TOC, and their isotopic distributions (Hanke et al., 2019; Itoh et al., 2012; Jiang et al., 2000), which are generally attributed to the co-migration characteristics of perylene and TOC in estuarine–coastal systems (Fang et al., 2016; Hu et al., 2014). Therefore, the JRE and MZCC are the two sources of surficial sedimentary TOC and co-migration perylene in the WTS.

The measured ^{14}C contents of TOC in the JRE ($\Delta^{14}C_{JRE\text{-}TOC}$) and WTS ($\Delta^{14}C_{WTS\text{-}TOC}$) are shown in Fig. 3 and Table S3. The ^{14}C contents of TOC in the surficial sediments of MZCC ($\Delta^{14}C_{MZCC\text{-}TOC}$) were reported as -431 ± 29‰ (Wu et al., 2013). Based on the ^{14}C end-member mixing model of TOC, the calculated fractional contributions of TOC and co-migration perylene from the JRE and MZCC (defined as f_{JRE} and f_{MZCC}, $f_{MZCC} = 1 - f_{JRE}$) to the WTS averaged $f_{JRE} = 47 \pm 8\%$ and $f_{MZCC} = 53 \pm 8\%$, respectively (Fig. 4c) (for the detailed calculation process, please *see* equations (5) and (6) in SI Text S5). This fractional contribution of perylene and TOC from the MZCC ($f_{MZCC} = 53 \pm 8\%$) was comparable to that of black carbon (~52%) (Wu et al., 2019b), which is one of the most important carriers of PAHs (Fang et al., 2016; Wu et al., 2019b). This further supports the use of perylene as a potential tracer for organic matter in marine environments (Zhang et al., 2014).

Furthermore, according to the ^{14}C end-member mixing model of perylene in the WTS (*see* equation (7) in SI Text S5), the ^{14}C content of perylene in the MZCC ($\Delta^{14}C_{MZCC\text{-}Per}$) can be estimated as -919 ± 53‰ (Fig. 4c), and the corresponding ^{14}C ages should be > 20,000 yr. The mud belt system of the MZCC is dynamically affected by the fluvial sources, of which the Yangtze River is the primary source (Liu et al., 2018). Therefore, the nearly ^{14}C-depleted perylene implies that sedimentary perylene from the MZCC underwent over ten thousand years of diagenesis before undergoing long-range transport to the WTS coast by inner shelf sediment transport processes. Owing to the coupled transport of coastal current-driven perylene and particle organic matter, the carbon age of perylene provides important geochemical information to reflect the time scale of fine-grained particle movement from the Yangtze River plume to the WTS driven by the south-westward MZCC.

Conclusions

The expanded application of CSRA reveals the advantages of the molecular-level ^{14}C approach in source appointment, especially for indicating the land–sea transport of PAHs. It can not only effectively avoid ambiguous PAH source results of the conventional methods but can also expand the object of source appointment to a single sample, and even a single PAH species. Our results show that fossil fuels (including direct input and combustion processes) contributed > 65% of medium/high-molecular-weight PAHs in the JRE and WTS sediment, and that the fractional contributions of fossil fuel and biomass burning to PAH species were different. In addition to the accurate source identification, the coherent variations of ^{14}C contents of PAH species and TOC from the JRE to WTS confirm that the ^{14}C signature can be used as a biogeochemical tracer of the land–sea transport of PAHs in estuarine–coastal sedimentary systems. In particular, for a significant biomarker in the source allocation of terrigenous organic matter (in this case perylene), the ^{14}C end-member mixing model provides an effective approach to quantitatively describe the land–sea transport of perylene from the basin through the estuary and finally to the coasts that are impacted by anthropogenic activities and coastal currents. Finally, the ^{14}C content is a useful geochemical tool for studying the transport and burial of organic pollutants in land–sea interfacial sediments. In the future, this approach will contribute to providing more organic geochemical information regarding multiphase partitioning,

multimedia migration interface transport, and the environmental fate of carbonaceous organic pollutants.

Declaration of Competing Interest

The authors declare no competing financial interest.

Acknowledgments

This work was supported by the National Natural Science Foundation of China (NSFC) Projects [grant numbers 41276066, 41877474]; and the China Scholarship Council (CSC). We sincerely thank the crew of the R/V Haiyang 2 and R/V Yanping 2 for sampling in the Jiulong River Estuary and the Western Taiwan Strait, respectively, and also thank the staff from the National Ocean Sciences Accelerator Mass Spectrometry facility of Woods Hole Oceanographic Institute for their support. We are grateful to the anonymous reviewers of our manuscript for their invaluable comments.

Supplementary materials

Supplementary material associated with this article can be found, in the online version, at doi:10.1016/j.watres.2021.117134.

References

Acquavita, A., Falomo, J., Predonzani, S., Tamberlich, F., Bettoso, N., Mattassi, G., 2014. The PAH level, distribution and composition in surface sediments from a Mediterranean Lagoon: the Marano and Grado Lagoon (Northern Adriatic Sea, Italy). Mar. Pollut. Bull. 81 (1), 234–241.

Bakhtiari, A.R., Zakaria, M.P., Yaziz, M.I., Lajis, M.N.H., Bi, X., Rahim, M.C.A, 2009. Vertical distribution and source identification of polycyclic aromatic hydrocarbons in anoxic sediment cores of Chini Lake, Malaysia: perylene as indicator of land plant-derived hydrocarbons. Appl. Geochem. 24 (9), 1777–1787.

Bao, R., McIntyre, C., Zhao, M., Zhu, C., Kao, S., Eglinton, T.I., 2016. Widespread dispersal and aging of organic carbon in shallow marginal seas. Geology 44 (10), 791–794.

Bertrand, O., Montarges-Pelletier, E., Mansuy-Huault, L., Losson, B., Faure, P., Michels, R., Pernot, A., Arnaud, F., 2013. A possible terrigenous origin for perylene based on a sedimentary record of a pond (Lorraine, France). Org. Geochem. 58, 69–77.

Bianchi, T.S., Allison, M.A., Cai, W., 2013. Biogeochemical Dynamics At Major River–Coastal interfaces: Linkages with Global Change. Cambridge University Press.

Bigus, P., Tobiszewski, M., Namieśnik, J., 2014. Historical records of organic pollutants in sediment cores. Mar. Pollut. Bull. 78 (1), 26–42.

Bosch, C., Andersson, A., Kruså, M., Bandh, C., Hovorková, I., Klánová, J., Knowles, T.D., Pancost, R.D., Evershed, R.P., Gustafsson, O., 2015. Source apportionment of polycyclic aromatic hydrocarbons in central european soils with compound-specific triple isotopes (δ^{13}C, Δ^{14}C, and δ^{2}H). Environ. Sci. Technol. 49 (13), 7657–7665.

Bouloubassi, I., Fillaux, J., Saliot, A., 2001. Hydrocarbons in surface sediments from the Changjiang (Yangtze River) estuary, East China Sea. Mar. Pollut. Bull 42 (12), 1335–1346.

Cai, Y., Wang, X., Wu, Y., Li, Y., Ya, M., 2016. Over 100-year sedimentary record of polycyclic aromatic hydrocarbons (PAHs) and organochlorine compounds (OCs) in the continental shelf of the East China Sea. Environ. Pollut. 219, 774–784.

Chen, H., Teng, Y., Wang, J., 2012. Source apportionment of polycyclic aromatic hydrocarbons (PAHs) in surface sediments of the Rizhao coastal area (China) using diagnostic ratios and factor analysis with nonnegative constraints. Sci. Total Environ. 414, 293–300.

Eglinton, T.I., Benitez-Nelson, B.C., Pearson, A., McNichol, A.P., Bauer, J.E., Druffel, E.R., 1997. Variability in radiocarbon ages of individual organic compounds from marine sediments. Science 277 (5327), 796–799.

Fang, Y., Chen, Y., Tian, C., Lin, T., Hu, L., Li, J., Zhang, G., 2016. Application of PMF receptor model merging with PAHs signatures for source apportionment of black carbon in the continental shelf surface sediments of the Bohai and Yellow Seas. China. J. Geophys. Res.: Oceans 121 (2), 1346–1359.

Fontenelle, F.R., Taniguchi, S., da Silva, J., Lourenço, R.A., 2019. Environmental quality survey of an industrialized estuary and an Atlantic Forest Biosphere Reserve through a comparative appraisal of organic pollutants. Environ. Pollut. 248, 339–348.

Gregg, T., Prahl, F.G., Simoneit, B.R., 2015. Suspended particulate matter transport of polycyclic aromatic hydrocarbons in the lower Columbia River and its estuary. Limnol. Oceanogr. 60 (6), 1935–1949.

Grice, K., Lu, H., Atahan, P., Asif, M., Hallmann, C., Greenwood, P., Maslen, E., Tulipani, S., Williford, K., Dodson, J., 2009. New insights into the origin of perylene in geological samples. Geochim. Cosmochim. Ac. 73 (21), 6531–6543.

Hanke, U.M., Lima-Braun, A.L., Eglinton, T.I., Donnelly, J.P., Galy, V., Poussart, P., Hughen, K., McNichol, A.P., Xu, L., Reddy, C.M., 2019. Significance of perylene for source allocation of terrigenous organic matter in aquatic sediments. Environ. Sci. Technol. 53 (14), 8244–8251.

Hu, L., Shi, X., Lin, T., Guo, Z., Ma, D., Yang, Z., 2014. Perylene in surface sediments from the estuarine-inner shelf of the East China Sea: a potential indicator to assess the sediment footprint of large river influence. Cont. Shelf Res. 90, 142–150.

Huh, C., Chen, W., Hsu, F., Su, C., Chiu, J., Lin, S., Liu, C., Huang, B., 2011. Modern (<100 years) sedimentation in the Taiwan Strait: rates and source-to-sink pathways elucidated from radionuclides and particle size distribution. Cont. Shelf Res. 31 (1), 47–63.

Ingalls, A.E., Pearson, A., 2005. Ten years of compound-specific radiocarbon analysis. Oceanography 18 (3), 18.

Inomata, Y., Kajino, M., Sato, K., Ohara, T., Kurokawa, J.I., Ueda, H., Tang, N., Hayakawa, K., Ohizumi, T., Akimoto, H., 2012. Emission and atmospheric transport of particulate PAHs in Northeast Asia. Environ. Sci. Technol. 46 (9), 4941–4949.

Itoh, N., Sakagami, N., Torimura, M., Watanabe, M., 2012. Perylene in Lake Biwa sediments originating from Cenococcum geophilum in its catchment area. Geochim. Cosmochim. Ac. 95, 241–251.

Jautzy, J.J., Ahad, J.M.E., Hall, R.I., Wiklund, J.A., Wolfe, B.B., Gobeil, C., Savard, M.M, 2015. Source apportionment of background PAHs in the Peace-Athabasca Delta (Alberta, Canada) using molecular level radiocarbon analysis. Environ. Sci. Technol. 49 (15), 9056–9063.

Jenkins, B.M., Jones, A.D., Turn, S.Q., Williams, R.B., 1996. Emission factors for polycyclic aromatic hydrocarbons from biomass burning. Environ. Sci. Technol. 30 (8), 2462–2469.

Jiang, C., Alexander, R., Kagi, R.I., Murray, A.P., 2000. Origin of perylene in ancient sediments and its geological significance. Org. Geochem. 31 (12), 1545–1559.

Kanke, H., Uchida, M., Okuda, T., Yoneda, M., Takada, H., Shibata, Y., Morita, M., 2004. Compound-specific radiocarbon analysis of polycyclic aromatic hydrocarbons (PAHs) in sediments from an urban reservoir. Nucl. Instrum. Meth. B 223, 545–554.

Katsoyiannis, A., Sweetman, A.J., Jones, K.C., 2011. PAH molecular diagnostic ratios applied to atmospheric sources: a critical evaluation using two decades of source inventory and air concentration data from the UK. Environ. Sci. Technol. 45 (20), 8897–8906.

Kumata, H., Uchida, M., Sakuma, E., Uchida, T., Fujiwara, K., Tsuzuki, M., Yoneda, M., Shibata, Y., 2006. Compound class specific ^{14}C analysis of polycyclic aromatic hydrocarbons associated with PM_{10} and $PM_{1.1}$ aerosols from residential areas of suburban Tokyo. Environ. Sci. Technol. 40 (11), 3474–3480.

Leorri, E., Mitra, S., Irabien, M.J., Zimmerman, A.R., Blake, W.H., Cearreta, A., 2014. A 700 year record of combustion-derived pollution in northern Spain: tools to identify the Holocene/Anthropocene transition in coastal environments. Sci. Total Environ. 470-471, 240–247.

Li, T., Sun, G., Ma, S., Liang, K., Yang, C., Li, B., Luo, W., 2016. Inferring sources of polycyclic aromatic hydrocarbons (PAHs) in sediments from the western Taiwan Strait through end-member mixing analysis. Mar. Pollut. Bull. 112 (1), 166–176.

Li, X., Zhang, Z., Wade, T.L., Knap, A.H., Zhang, C.L., 2017. Sources and compositional distribution of organic carbon in surface sediments from the lower Pearl River to the coastal South China Sea. J. Geophys. Res.: Biogeo. 122 (8), 2104–2117.

Li, Y., Liu, M., Hou, L., Li, X., Yin, G., Sun, P., Yang, J., Wei, X., He, Y., Zheng, D, 2021. Geographical distribution of polycyclic aromatic hydrocarbons in estuarine sediments over China: human impacts and source apportionment. Sci. Total Environ. 768, 145279.

Lin, T., Hu, L., Guo, Z., Zhang, G., Yang, Z., 2013. Deposition fluxes and fate of polycyclic aromatic hydrocarbons in the Yangtze River estuarine-inner shelf in the East China Sea. Global. Biogeochem. Cy. 27 (1), 77–87.

Liu, J.T., Hsu, R.T., Yang, R.J., Wang, Y., Wu, H., Du, X., Li, A., Chien, S.C., Lee, J., Yang, S., Zhu, J., Su, C., Chang, Y., Huh, C., 2018. A comprehensive sediment dynamics study of a major mud belt system on the inner shelf along an energetic coast. Sci. Rep. 8 (1), 4229.

Liu, L.Y., Wang, J.Z., Wei, G.L., Guan, Y.F., Zeng, E.Y., 2012. Polycyclic aromatic hydrocarbons (PAHs) in continental shelf sediment of China: implications for anthropogenic influences on coastal marine environment. Environ. Pollut. 167, 155–162.

Liu, X., Liu, M., Zhou, L., Hou, L., Yang, Y., Wu, D., Meadows, M.E., Li, Z., Tong, C., Gu, J., 2021. Occurrence and distribution of PAHs and microbial communities in nearshore sediments of the Knysna Estuary. South Africa. Environ. Pollut. 270, 116083.

Lu, G., Dang, Z., Tao, X., Peng, P., Zhang, D, 2005. QSPR study on direct photolysis half-lives of PAHs in water surface. J. Theor. Comput. Chem. 04 (03), 811–822.

Lu, Y., Wang, Q.g., Zhang, X., Qian, Y., Qian, X., 2019. China's black carbon emission from fossil fuel consumption in 2015, 2020, and 2030. Atmos. Environ. 212, 201–207.

Mandalakis, M., Gustafsson, O., Alsberg, T., Egebäck, A.L., Reddy, C.M., Xu, L., Klanova, J., Holoubek, I., Stephanou, E.G., 2005. Contribution of biomass burning to atmospheric polycyclic aromatic hydrocarbons at three European background sites. Environ. Sci. Technol. 39 (9), 2976–2982.

Mandalakis, M., Gustafsson, Ö., Reddy, C.M., Xu, L., 2004a. Radiocarbon apportionment of fossil versus biofuel combustion sources of polycyclic aromatic hydrocarbons in the Stockholm metropolitan area. Environ. Sci. Technol. 38 (20), 5344–5349.

Mandalakis, M., Zebühr, Y., Gustafsson, Ö., 2004b. Efficient isolation of polyaromatic fraction from aliphatic compounds in complex extracts using dimethylformamide-pentane partitionings. J. Chromatogr. A 1041 (1), 111–117.

Martins, C.C., Bícego, M.C., Mahiques, M.M., Figueira, R.C.L., Tessler, M.G., Montone, R.C, 2011. Polycyclic aromatic hydrocarbons (PAHs) in a large South American industrial coastal area (Santos Estuary, Southeastern Brazil): sources and depositional history. Mar. Pollut. Bull. 63 (5), 452–458.
Marynowski, L., Smolarek, J., Bechtel, A., Philippe, M., Kurkiewicz, S., Simoneit, B.R.T, 2013. Perylene as an indicator of conifer fossil wood degradation by wood-degrading fungi. Org. Geochem. 59, 143–151.
Maskaoui, K., Zhou, J., Hong, H., Zhang, Z., 2002. Contamination by polycyclic aromatic hydrocarbons in the Jiulong River Estuary and Western Xiamen Sea. China. Environ. Pollut. 118 (1), 109–122.
Niu, Z., Zhou, W., Wu, S., Cheng, P., Lu, X., Xiong, X., Du, H., Fu, Y., Wang, G., 2016. Atmospheric fossil fuel CO_2 traced by $\Delta^{14}C$ in Beijing and Xiamen, China: temporal variations, inland/coastal differences and influencing factors. Environ. Sci. Technol. 50 (11), 5474–5480.
Pearson, A., McNichol, A.P., Schneider, R.J., Von Reden, K.F., Zheng, Y., 1997. Microscale AMS ^{14}C measurement at NOSAMS. Radiocarbon 40 (1), 61–75.
Pichler, N., Maria de Souza, F., Ferreira dos Santos, V., Martins, C.C., 2021. Polycyclic aromatic hydrocarbons (PAHs) in sediments of the amazon coast: evidence for localized sources in contrast to massive regional biomass burning. Environ. Pollut. 268, 115958.
Pozo, K., Perra, G., Menchi, V., Urrutia, R., Parra, O., Rudolph, A., Focardi, S., 2011. Levels and spatial distribution of polycyclic aromatic hydrocarbons (PAHs) in sediments from Lenga Estuary, central Chile. Mar. Pollut. Bull. 62 (7), 1572–1576.
Rauert, C., Harner, T., Ahad, J.M.E., Percy, K.E, 2020. Using tree cores to evaluate historic atmospheric concentrations and trends of polycyclic aromatic compounds in the Oil Sands region of Alberta. Canada. Sci. Total Environ. 739, 139996.
Santos, F.R., Neves, P.A., Kim, B.S.M., Taniguchi, S., Lourenço, R.A., Timoszczuk, C.T., Sotão, B.M.T., Montone, R.C., Figueira, R.C.L., Mahiques, M.M., Bícego, M.C, 2020. Organic contaminants and trace metals in the western South Atlantic upper continental margin: anthropogenic influence on mud depocenters. Mar. Pollut. Bull. 154, 111087.
Santschi, P.H., Guo, L., Asbill, S., Allison, M., Britt Kepple, A., Wen, L.S., 2001. Accumulation rates and sources of sediments and organic carbon on the Palos Verdes shelf based on radioisotopic tracers (^{137}Cs, $^{239,240}Pu$, ^{210}Pb, ^{234}Th, ^{238}U and ^{14}C). Mar. Chem. 73 (2), 125–152.
Shah, S.R., Pearson, A., 2007. Ultra-microscale (5-25 μg C) analysis of individual lipids by ^{14}C AMS: assessment and correction for sample processing blanks. Radiocarbon 49 (1), 69–82.
Sheesley, R.J., Krusà, M., Krecl, P., Johansson, C., Gustafsson, Ö., 2009. Source apportionment of elevated wintertime PAHs by compound-specific radiocarbon analysis. Atmos. Chem. Phys. 9 (10), 3347–3356.
Silliman, J.E., Meyers, P.A., Ostrom, P.H., Ostrom, N.E., Eadie, B.J., 2000. Insights into the origin of perylene from isotopic analyses of sediments from Saanich Inlet. British Columbia. Org. Geochem. 31 (11), 1133–1142.
Slater, G., Benson, A., Marvin, C., Muir, D, 2013. PAH fluxes to Siskiwit revisted: trends in fluxes and sources of pyrogenic PAH and perylene constrained via radiocarbon analysis. Environ. Sci. Technol. 47 (10), 5066–5073.
Stuiver, M., Polach, H.A., 1977. Discussion reporting of ^{14}C data. Radiocarbon 19 (3), 355–363.
Sutilli, M., Ferreira, P.A.L., Figueira, R.C.L., Martins, C.C, 2019. Depositional input of hydrocarbons recorded in sedimentary cores from Deception and Penguin Islands (South Shetland Archipelago. Antarctica). Environ. Pollut. 253, 981–991.
Suzuki, N., Yessalina, S., Kikuchi, T., 2010. Probable fungal origin of perylene in Late Cretaceous to Paleogene terrestrial sedimentary rocks of northeastern Japan as indicated from stable carbon isotopes. Org. Geochem. 41 (3), 234–241.
Tang, T., Cheng, Z., Xu, B., Zhang, B., Zhu, S., Cheng, H., Li, J., Chen, Y., Zhang, G., 2020. Triple isotopes ($\delta^{13}C$, $\delta^{2}H$, and $\Delta^{14}C$) compositions and source apportionment of atmospheric naphthalene: a key surrogate of intermediate-volatility organic compounds (IVOCs). Environ. Sci. Technol. 54 (9), 5409–5418.
Tobiszewski, M., Namieśnik, J., 2012. PAH diagnostic ratios for the identification of pollution emission sources. Environ. Pollut. 162, 110–119.
Vane, C.H., Chenery, S.R., Harrison, I., Kim, A.W., Moss-Hayes, V., Jones, D.G., 2011. Chemical signatures of the Anthropocene in the Clyde estuary, UK: sediment-hosted Pb, $^{207/206}Pb$, total petroleum hydrocarbon, polyaromatic hydrocarbon and polychlorinated biphenyl pollution records. Philos. T. R. Soc. A 369 (1938), 1085–1111.
Varnosfaderany, M.N., Bakhtiari, A.R., Gu, Z., Chu, G., 2014. Perylene as an indicator of land-based plant biomarkers in the southwest Caspian Sea. Mar. Pollut. Bull. 80 (1), 124–131.
Venkatesan, M.I., 1988. Occurrence and possible sources of perylene in marine sediments: a review. Mar. Chem. 25 (1), 1–27.
Wang, D., Zheng, Q., Hu, J., 2013. Jet-like features of Jiulongjiang River plume discharging into the west Taiwan Strait. Front. Earth Sci. 7 (3), 282–294.
Wang, Y., Li, T., Zhang, R., Russell, J., Xiao, X., Cheng, Y., Zhang, F., Liu, Z., Guan, M., Han, Q., 2020. Fingerprinting characterization of sedimentary PAHs and black carbon in the East China Sea using carbon and hydrogen isotopes. Environ. Pollut. 267, 115415.
Wang, Y., Shen, C., Shen, Z., Zhang, D., Crittenden, J.C., 2015. Spatial variation and sources of polycyclic aromatic hydrocarbons (PAHs) in surface sediments from the Yangtze Estuary. China. Environ. Sci.: Proc. Imp. 17 (7), 1340–1347.
Wu, Y., Eglinton, T., Yang, L., Deng, B., Montluçon, D., Zhang, J., 2013. Spatial variability in the abundance, composition, and age of organic matter in surficial sediments of the East China Sea. J. Geophys. Res.: Biogeo. 118 (4), 1495–1507.
Wu, Y., Wang, X., Li, Y., Hong, H., 2011. Occurrence of polycyclic aromatic hydrocarbons (PAHs) in seawater from the Western Taiwan Strait, China. Mar. Pollut. Bull. 63 (5), 459–463.
Wu, Y., Wang, X., Ya, M., Li, Y., Hong, H., 2016. Distributions of organochlorine compounds in sediments from Jiulong River Estuary and adjacent Western Taiwan Strait: implications of transport, sources and inventories. Environ. Pollut. 219, 519–527.
Wu, Y., Wang, X., Ya, M., Li, Y., Hong, H., 2019a. Seasonal variation and spatial transport of polycyclic aromatic hydrocarbons in water of the subtropical Jiulong River watershed and estuary. Southeast China. Chemosphere 234, 215–223.
Wu, Y., Ya, M., Chen, H., Li, Y., Guo, W., Wang, X., 2019b. Distribution and isotopic composition of sedimentary black carbon in a subtropical estuarine-coastal region of the western Taiwan Strait: implications for tracing anthropogenic inputs. Sci. Total Environ. 684, 509–518.
Xu, L., Zheng, M., Ding, X., Edgerton, E.S., Reddy, C.M., 2012. Modern and fossil contributions to polycyclic aromatic hydrocarbons in $PM_{2.5}$ from North Birmingham. Alabama in the Southeastern U.S. Environ. Sci. Technol. 46 (3), 1422–1429.
Ya, M., Wang, X., Wu, Y., Li, Y., Yan, J., Fang, C., Zhao, Y., Qian, R., Lin, X., 2017a. Seasonal variation of terrigenous polycyclic aromatic hydrocarbons along the marginal seas of China: input, phase partitioning, and ocean-current transport. Environ. Sci. Technol. 51 (16), 9072–9079.
Ya, M., Wu, Y., Li, Y., Wang, X., 2017b. Transport of terrigenous polycyclic aromatic hydrocarbons affected by the coastal upwelling in the northwestern coast of South China Sea. Environ. Pollut. 229, 60–68.
Ya, M., Wu, Y., Wang, X., Li, Y., Su, G., 2020. The importance of compound-specific radiocarbon analysis in source identification of polycyclic aromatic hydrocarbons: a critical review. Crit. Rev. Env. Sci. Tec. 1–42.
Ya, M., Xu, L., Wu, Y., Li, Y., Zhao, S., Wang, X., 2018. Fossil fuel-derived polycyclic aromatic hydrocarbons in the Taiwan Strait, China, and fluxes across the air-water interface. Environ. Sci. Technol. 52 (13), 7307–7316.
Yu, M., Guo, Z., Wang, X., Eglinton, T.I., Yuan, Z., Xing, L., Zhang, H., Zhao, M., 2018. Sources and radiocarbon ages of aerosol organic carbon along the east coast of China and implications for atmospheric fossil carbon contributions to China marginal seas. Sci. Total Environ 619-620, 957–965.
Yunker, M.B., Macdonald, R.W., Vingarzan, R., Mitchell, R.H., Goyette, D., Sylvestre, S., 2002. PAHs in the Fraser River basin: a critical appraisal of PAH ratios as indicators of PAH source and composition. Org. Geochem. 33 (4), 489–515.
Zencak, Z., Klanova, J., Holoubek, I., Gustafsson, Ö., 2007. Source apportionment of atmospheric PAHs in the Western Balkans by natural abundance radiocarbon analysis. Environ. Sci. Technol. 41 (11), 3850–3855.
Zhang, C., Lin, Y., 2012. Panel estimation for urbanization, energy consumption and CO2 emissions: a regional analysis in China. Energ. Policy 49, 488–498.
Zhang, X.L., Tao, S., Liu, W.X., Yang, Y., Zuo, Q., Liu, S.Z., 2005. Source diagnostics of polycyclic aromatic hydrocarbons based on species ratios: a multimedia approach. Environ. Sci. Technol. 39 (23), 9109–9114.
Zhang, X.Y., Xu, Y.P., Ruan, J.P., Ding, S., Huang, X.Y., 2014. Origin, distribution and environmental significance of perylene in Okinawa Trough since last glaciation maximum. Org. Geochem. 76, 288–294.
Zhou, J.L., Hong, H., Zhang, Z., Maskaoui, K., Chen, W., 2000. Multi-phase distribution of organic micropollutants in Xiamen Harbour. China. Water Res. 34 (7), 2132–2150.